Research, Society and Development, v. 11, n. 14, e109111436004, 2022
(CC BY 4.0) | ISSN 2525-3409 | DOI: http://dx.doi.org/10.33448/rsd-v11i14.36004

Green synthesis of Fe_3O_4@ZnO-supported Pd nanoparticles for oxidation and hydrogenation reactions in liquid systems

Síntese verde de nanopartículas de Pd suportadas em Fe_3O_4@ZnO para reações de oxidação e hidrogenação em sistemas líquidos

Síntesis verde de nanopartículas de Pd soportadas en Fe3O4@ZnO para reacciones de oxidación e hidrogenación en sistemas líquidos

Received: 09/30/2022 | Revised: 10/13/2022 | Accepted: 10/15/2022 | Published: 10/21/2022

Robson Da Silva Souto
ORCID: https://orcid.org/0000-0001-9142-0665
Universidade Federal de Mato Grosso, Brazil
E-mail: robsonssouto@gmail.com
Samara Da Silva Razini
ORCID: https://orcid.org/0000-0001-5626-2155
Universidade Federal de Mato Grosso, Brazil
E-mail: samararazini95@gmail.com
Angélica Correa Kauffmann
ORCID: https://orcid.org/0000-0003-1582-4435
Universidade Federal de Mato Grosso, Brazil
E-mail: angelicakauffmann@hotmail.com
Virgínia Claudia Paulino Silva
ORCID: https://orcid.org/0000-0002-4563-0394
Universidade Federal de São Carlos, Brazil
E-mail: vcsvirginia@gmail.com
Paulo Teixeira de Sousa Jr
ORCID: https://orcid.org/0000-0002-6086-1502
Universidade Federal de Mato Grosso, Brazil
E-mail: pauloteixeiradesousa@gmail.com
Andris Bakuzis
ORCID: https://orcid.org/0000-0003-3366-106X
Universidade Federal de Goiás, Brazil
E-mail: abakuzis@gmail.com
Luis Cesar Fontana
ORCID: https://orcid.org/0000-0003-0751-1711
Universidade do Estado de Santa Catarina, Brazil
E-mail: luis.fontana@udesc.br
Marcos José Jacinto
ORCID: https://orcid.org/0000-0002-7182-9735
Universidade Federal de Mato Grosso, Brazil
E-mail: marcjrd@hotmail.com

Abstract

In this work Pd nanoparticles immobilized on a hybrid solid support comprised of Fe_3O_4 coated by a ZnO layer were synthesized by a green method which makes use of water, a biological substrate from a local plant (*Rhamnidium elaeocarpum*) and inexpensive Fe^{3+} and Zn^{2+} salts. ^{1}H-NMR and 13C-NM revealed β-sitosterol as the main component of the biological substrate. The catalytic support containing Pd nanoparticles was applied in three model solid-liquid catalytic systems, namely: alcohol oxidation, nitrocompound reduction and olefin hydrogenation. For the alcohol oxidation, benzyl alcohol was used as the substrate in a solvent-free condition with high selectivity towards benzaldehyde, and a single sample of the catalyst could be recycled up to 11 times before any loss of activity could be detected. TOF (turnover frequency) as high as 13,686 h^{-1} for the substrate oxidation was achieved with an average yield rate of 45.4% for formation of benzaldehyde and 81.6% of average substrate conversion after 6 catalytic cycles. For the hydrogenation experiments using cyclohexene and 4-nitrophenol as model substrates, conversion as high as 96% to 4-aminophenol and cyclohexane, respectively, was achieved after 30 minutes of reaction. Furthermore, a single sample of the catalyst could be recycled for up to 17 times for the reduction of 4-nitrophenol, and 21 times in the hydrogenation of cyclohexene. Catalytic recycling for all studied reactions was straightforward after due to the superparamagnetic property of the material, and catalyst isolation after each batch could be rapidly carried out using a Nd magnet. These results suggests that a highly active and stable catalytic system based on Pd nanoparticles

supported on a multifunctional solid could be fabricated using green and inexpensive biomass under operationally simple synthesis conditions.
Keywords: Nanomaterials; Magnetic separation; Biosynthesis.

Resumo

Neste trabalho, nanopartículas de Pd imobilizadas em um suporte sólido híbrido composto de Fe_3O_4 revestido por uma camada de ZnO foram sintetizadas por um método verde que utiliza água, um substrato biológico de uma planta local (Rhamnidium elaeocarpum) e sais metálicos de Fe^{3+} e Zn^{2+}. 1H-NMR e 13C-NM revelaram o β-sitosterol como o principal componente do substrato biológico. O suporte catalítico contendo nanopartículas de Pd foi aplicado em três modelos de sistemas catalíticos sólido-líquido, a saber: oxidação de álcool, redução de nitrocompostos e hidrogenação de olefinas. Para a oxidação do álcool, o álcool benzílico foi usado como substrato em uma condição livre de solvente, com alta seletividade em relação ao benzaldeído, e uma única amostra do catalisador pôde ser reciclada até 11 vezes antes que qualquer perda de atividade pudesse ser detectada. TOF (frequência de rotatividade) de 13.686 h-1 para a oxidação do substrato foi alcançado com uma taxa média de rendimento de 45,4% para a formação de benzaldeído e 81,6% de conversão média do substrato após 6 ciclos catalíticos. Para os experimentos de hidrogenação usando ciclohexeno e 4-nitrofenol como substratos modelo, a conversão foi de 96% para 4-aminofenol e ciclohexano, respectivamente, após 30 minutos de reação. Além disso, uma única amostra do catalisador pôde ser reciclada por até 17 vezes para a redução do 4-nitrofenol, e 21 vezes na hidrogenação do ciclohexeno. A reciclagem catalítica para todas as reações estudadas foi realizada de forma simples devido à propriedade superparamagnética do material, e o isolamento do catalisador após cada lote pôde ser realizado rapidamente usando um ímã de Nd. Esses resultados sugerem que um sistema catalítico altamente ativo e estável baseado em nanopartículas de Pd suportadas em um sólido multifuncional pode ser fabricado usando biomassa verde e barata em condições de síntese operacionalmente simples.
Palavras-chave: Nanomateriais; Separação magnética; Biossíntese.

Resumen

En este trabajo se sintetizaron nanopartículas de Pd inmovilizadas sobre un soporte sólido híbrido compuesto por Fe3O4 recubierto con una capa de ZnO mediante un método verde que utiliza agua, un sustrato biológico de una planta local (Rhamnidium elaeocarpum) y sales metálicas de Fe3+ y Zn2+. 1H-NMR y 13C-NM revelaron β-sitosterol como componente principal del sustrato biológico. El soporte catalítico que contiene nanopartículas de Pd se aplicó en tres modelos de sistemas catalíticos sólido-líquido, a saber: oxidación de alcoholes, reducción de nitrocompuestos e hidrogenación de olefinas. Para la oxidación del alcohol, se usó alcohol bencílico como sustrato en una condición libre de solventes, con alta selectividad hacia el benzaldehído, y una sola muestra del catalizador se pudo reciclar hasta 11 veces antes de que se pudiera detectar cualquier pérdida de actividad. Se logró un TOF (frecuencia de rotación) de 13 686 h-1 para la oxidación del sustrato con una tasa de rendimiento promedio del 45,4 % para la formación de benzaldehído y una conversión promedio del sustrato del 81,6 % después de 6 ciclos catalíticos. Para los experimentos de hidrogenación utilizando ciclohexeno y 4-nitrofenol como sustratos modelo, la conversión fue del 96 % para 4-aminofenol y ciclohexano, respectivamente, después de 30 minutos de reacción. Además, una sola muestra del catalizador podría reciclarse hasta 17 veces para la reducción de 4-nitrofenol y 21 veces para la hidrogenación de ciclohexeno. El reciclaje catalítico de todas las reacciones estudiadas se realizó de forma sencilla debido a la propiedad superparamagnética del material, y el aislamiento del catalizador después de cada lote se pudo realizar rápidamente utilizando un imán de Nd. Estos resultados sugieren que se puede fabricar un sistema catalítico altamente activo y estable basado en nanopartículas de Pd soportadas en un sólido multifuncional utilizando biomasa verde barata en condiciones de síntesis operativamente simples.
Palabras clave: Nanomateriales; Separación magnética; Biosíntesis.

1. Introduction

Green chemistry aims to develop chemical products and processes that seek to reduce or eliminate the use and generation of hazardous substances. Catalysis is a well-known green chemistry principle, and it recommends the use of catalytic reagents rather than stoichiometric reagents that exhibit poor selectivity and pollute our environment (Miceli et al., 2021). In view of this, researchers have focused on developing more ecological and cost-effective catalytic processes which has largely impacted the concept and design of catalytic materials. One approach that has begun to emerge as a greener alternative for the fabrication of nanosctructured catalytic architectures is the use of biological substrates (BS) as both the reducing and stabilizing agents normally required in the synthesis of nanomaterials as substitutes for harmful precursors including surfactants, organometallic compounds, metal hydrides and so forth (Camargo et al., 2009; Ma et al., 2019; Vieira et

al., 2020). In heterogeneous solid-liquid catalytic systems, the use of magnetic nanocomposites as support allows an easy dispersion in the reaction medium and a quick recovery and recycling of the catalyst when compared to the commonly used centrifugation or filtration processes (Miceli et al., 2021). Among the main types of magnetic nanocomposites widely used in heterogeneous catalysis, metallic oxide-based matrices has stood out, mostly due to considerable gains in terms of thermal, chemical, and adsorption stability, in addition to the magnetic, electronic, and optical properties that this type of material exhibits (Camargo et al., 2009). Magnetite (Fe_3O_4) is an example of iron oxide that shows a considerate enhanced magnetism, defined as superparamagnetism, when one of its dimensions are reduced to the nanoscale. Thus, Fe_3O_4 nanoparticles have been utilized as catalyst/support and co-catalyst in a variety of reactions including Fenton-type oxidations, Hydrogenation of arenes and olefins, Oxidation of alcohols/olefins and nitro compound reduction (Ma et al., 2019; Vieira et al., 2020). In the past decade, the use of zinc oxide in the fabrication of magnetic core@shell structures has increased remarkably (Ammar et al., 2020; Wang et al., 2016; Wu et al., 2012). This is mainly attributed to the semiconducting property of ZnO and to the fact that it is much cheaper than TiO_2 (Bahtiar et al., 2019). However, ZnO is also a promising candidate for support material in the fabrication of other solid-liquid catalytic systems such as oxidation, hydroformylation and hydrogenation. Besides the advantages previously mentioned, Metal-Zn alloy can improve the reaction selectivity towards specific products as has been reported by Bahruji et al. where it was showed that PdZn bimetallic formation was responsible for the high selectivity to methanol production in the hydrogenation of CO2 (Bahruji et al., 2016). Alcohol oxidation is widely used for the production of paints, plastics, detergents, food additives, cosmetics, and drug intermediates (Mallat & Baiker, 2004). Hydrogenation reactions can serve both for the synthesis of products and the neutralization of harmful compounds. An example is a conversion of nitro compounds into amino compounds, a process broadly used for the manufacture of anticorrosive lubricant, hair drying agent, corrosion inhibitor, photographic developer, and a well-known intermediate in the synthesis of antipyretic and analgesic drugs (Shanmugam et al., 2019). Similarly, the reduction of alkene compounds for the petrochemical industry can be used to saturate alkene, alkyne, and aromatic compounds, and the products of such process are widely used in pharmaceutical and petrochemical syntheses (Yu et al., 2020). Due to their specific characteristics, supported transition metals are considered excellent candidates for application in catalytic processes that require an oxidation/reduction step. Palladium is a transition metal commonly used for, alkene isomerization (Chuc et al., 2017) and hydrogenation (Kuai et al., 2020), oxidations (Guo et al., 2019), and carbon-carbon cross-coupling reactions (Parmanand et al., 2019). In this work, we present a method of direct biosynthesis of magnetic supported Pd nanoparticles, using bark/stem extract of *Rhamnidium elaeocarpum* Reissek (Rhamnaceae) species. The Pd nanoparticles, with an average size of 21.9 nm, were deposited on a magnetic nanocomposite (Fe_3O_4@ZnO) used as a support. The Fe_3O_4@ZnO-Pd catalyst was characterized by analysis of XPS, EDX, TEM, and VSM, and the composition of the plant extract was evaluated by 1H, 13C NMR and FTIR. The efficiency and stability of the catalyst was examined in the benzyl-alcohol solvent-free oxidation and hydrogenation of 4-nitrophenol and cyclohexene. Under the conditions studied, a single sample of the catalyst could be recycled for 11 times before any deactivation could be observed. For the oxidation experiments, TOF values as high as 13 686 h^{-1} was observed, with an average yield rate of 45.4% up to the 8th cycle. In addition, an average conversion of 81.6% after 6 catalytic cycles could be achieved. For the hydrogenation reactions of 4-nitrophenol and cyclohexene, conversion values higher than 96% was achieved after 30 minutes. The catalyst recycling studies allowed the use of a single catalytic sample up to 17 times for cyclohexene and 21 times for 4-nitrophenol. 1H and 13C NMR confirmed that beta-Sitosterol is the main component of the acetate fraction used in the synthesis of Pd nanoparticles. We believe the biosynthetic protocol applied in the multi-step synthesis of the hybrid material provided with multifunctional properties such as catalytic capability and superparamagnetism is essential is of great importance in the search for eco-friendly, efficient and inexpensive synthesis of nanomaterials.

2. Methodology

2.1 Preparation of Plant Extract

Fresh bark/stem of *Rhamnidium elaeocarpum* were collected in Poconé, Mato Grosso, Brazil (16°28'7.1''S 057°02'0.32''W). The material was dried for a week under environmental conditions, with no sun exposure, and crushed using a knife mill. In order to obtain the ethyl acetate fraction of the bark/stem for the biosynthesis of palladium nanoparticles, the crude ethanol extract of the bark/stem was subjected to solid-liquid partition using 70-230 mesh silica gel as stationary phase and eluted with ethyl acetate (3.5 L). Then, the obtained extract was filtered and concentrated using a rotary evaporator under reduced pressure.

2.2 Biosynthesis of magnetic core and coating by ZnO.

The biosynthesis of Fe_3O_4, used as the magnetic core for the catalyst, is described in detail by previously published work (Jacinto et al., 2021). Summarizing, 600 mg of $FeCl_3.6H_2O$ and 2.00 g of urea were added to a Fisher-Porter reactor followed by the addition of 15 ml of an aqueous solution containing the ethanolic bark extract (1.06 $g.ml^{-1}$) of *R. elaeocarpum*. The mixture was kept under magnetic stirring in the reactor, which was autoclaved and held at 150 °C for two hours. After the solution was cooled down, the magnetic nanoparticles were collected using a Nd magnet, and the material was washed twice with water/ethanol, to remove unreacted precursors, and dried at 70 °C for one hour using a vacum pump air. The coating of the magnetic core (Fe_3O_4) by a mesoporous zinc oxide layer was carried out by a modified procedure described previously (da Silva et al., 2018). In summary, 100 mg Fe_3O_4 was added to a 100 ml flask containing an aqueous solution of zinc acetate (5 $g.l^{-1}$). Then, 5.00 g of urea and 2.00 g of CTAB (cetyltrimethylammonium bromide) were added to the flask, and the mixture was kept under magnetic stirring (500 rpm) at 85 °C for eight hours. The material was then magnetically isolated, washed with water and acetone and dried in a vacuum pump at 60 °C for one hour. The solid was labeled as Fe_3O_4@ZnO.

2.3 Biosynthesis of palladium nanoparticles

In this step, 700 mg of the ethyl acetate fraction solution from the bark/stem of *R. elaeocarpum* (44.4 $g.l^{-1}$) was added to a three-neck flask containing 29 mL of a palladium nitrate aqueous solution (0.6 $mg.mL^{-1}$). The mixture was placed under magnetic stirring for eight hours at 70°C.

2.4 Deposition of Pd^0 nanoparticles in support

In this step, 400 mg of the Fe_3O_4@ZnO support were added to the flask containing the as-synthesized Pd nanoparticles. The mixture was kept under magnetic stirring for 24 hours, and then magnetically isolated, and washed twice with water/ethanol and dried in a vacuum pump at 80 °C for one hour. The material was labeled Fe_3O_4@ZnO-Pd

2.5 Instruments

The composition profile of the ethyl acetate fraction of *R. elaeocarpum* was investigated by FTIR using a Shimadzu Iraffinity-1 and by RMN using a BRUKER AscendTM Nuclear Magnetic Resonance spectrometers, 500 MHz for H and 125 MHz for ^{13}C). The analysis of the composition and energy states of the surface of the material was carried out by X-ray photoelectron spectroscopy (XPS), performed on a Thermo Scientific spectrometer which utilizes Aluminum K-alpha X-rays (1486.6 eV). High resolution spectra for selected elements were obtained using a pass energy of 44 eV. In order to assess the magnetization properties of the materials, room-temperature magnetization curves were measured using a commercial vibrating sample magnetometer (ADE-Magnetics, model: EV9) with field range±2 T. Morphology and composition were

analyzed by Transmission electron microscopy (TEM), high-resolution transmission electron microscopy (HRTEM) and X-ray energy dispersive spectroscopy (EDS). These techniques were carried out using a FEI TECNAI F20 electron microscope operating at 200 kV. For analysis of product reactions of oxidation and hydrogenation of cyclohexene, we use the Shimadzu LC-20AT model, coupled to a Shimadzu SPD-M20A diode array detector. The chromatography method used was the stationary phase: C-18 reverse phase, methanol-water mobile phase (70/30), isocratic elution mode with a flow of 1.0 mL/min, column temperature of 40 ºC, volume injection of 10 µL, and run time of 10 minutes. For hydrogenation analysis of 4-nitrophenol we use UV-Vis spectrophotometer, KASUAKI® brand, in a wavelength range between 200-500 nm, with quartz cuvettes of 1x1 cm as an optical medium.

2.6 Catalytic set-up

The catalytic tests were carried out in a modified Fischer-Porter reactor. For each batch, a target amount of catalyst/substrate was added to the reactor vessel which was purged with vacuum and pressurized with either O_2 for the oxidation reactions or H_2 for the hydrogenation experiments at the established temperature, pressure and reaction time. After the selected reaction time, the catalyst was magnetically isolated using an Nd magnet (4000 G), and a liquid sample was removed for analysis using a syringe. For the oxidation test, 1 mL of benzyl alcohol (BzOH) in solventless conditions was used as a model substrate. In order to evaluate the course of the oxidation reaction, 5.0 µl aliquots were removed from each batch and diluted in 50 mL of a methanol/water solution (70/30). The prepared samples were analyzed by HPLC-DAD device, and peaks corresponding to BzOH at 210 nm and benzaldehyde reaction at 250 nm were monitored.

For the catalytic hydrogenation tests, cyclohexene, in solventless conditions, and an aqueous solution of 4-Nitrophenol (13 $mg.ml^{-1}$) were used as substrates for the olefin and nitro compound hydrogenation, respectively. In order to evaluate the cyclohexene reduction, 4.0 µl aliquots were removed from the solution and diluted in 25 ml of methanol p.a. Substrate conversion to the saturated form was analyzed by monitoring the intensity of the cyclohexene peak at 230 nm. In order to evaluate the conversion of 4-nitrophenol (4-NP) to 4-aminophenol by UV-VIS spectrophotometry, a liquid sample (15 µl) was withdrawn from the reactor at the established time and added to a 25 mL of ammonium hydroxide (pH = 11).

The catalytic efficiency was determined by the total turnonver number (TTON) and turnover frequency (TOF) which were calculated by the equations:

$$TON = \frac{\text{mols of substrate}}{\text{mols of catalyst}} \quad \text{(eq. 1)}$$

$$TOF = \frac{\text{TON of 1}^{\circ}\text{ batch}}{\text{time reaction (h)}} \quad \text{(eq. 2)}$$

The number of mols of catalyst (Pd) was calculated using the mass percentage of Pd obtained by XRF (0.88 %).

3. Results and Discussion

FTIR and NMR were used to elucidate the composition of the ethyl acetate extract used in the fabrication of the supported Pd nanoparticles. FTIR spectrum (Figure 1A) shows an absorption range between 3500-3000 cm^{-1}, commonly associated with O-H stretching from molecules containing polyphenols, alcohols, and carboxylic groups (Ododo et al., 2016). Besides, well-defined peaks are observed at wavelengths 1606 and 1061 cm^{-1}, which can be related to the presence of unconjugated olefinic groups (C=C) and secondary alcohols (O-H), respectively. Other smaller peaks at 1445 and 1360 cm^{-1} are associated with cyclic methylene (CH_2) and gem-dimethyl ($-CH(CH_3)_2$) groups, respectively (López-Salazar et al., 2019).

Figure 1B exhibits the ^{1}H-NMR (500 MHz, Pyridine-d5) spectra profile of the ethyl acetate extract. The high-field region between δ_H 0.67 to 2.77 corresponds to aliphatic hydrogen that are characteristic of a steroidal skeleton. The spectrum also reveals signals at δH 4,59 (1H), 4,44 (1H), 4,32 (2H), 4,09 (1H) e 4,00 (2H) that are typical of a glycosidic unit. This is corroborated by the presence of a duplet at δH 5,07 (d; J=7,5 Hz, 1H) that is attributed to H-1'from a glucose unit in beta linkages (Munvera et al., 2021; Raimundo & Silva et al., 2020).

Figure 1. FTIR spectra (1A) and H^{1}NMR (1B) of the ethyl acetate extract from *Rhamnidium elaeocarpum*.

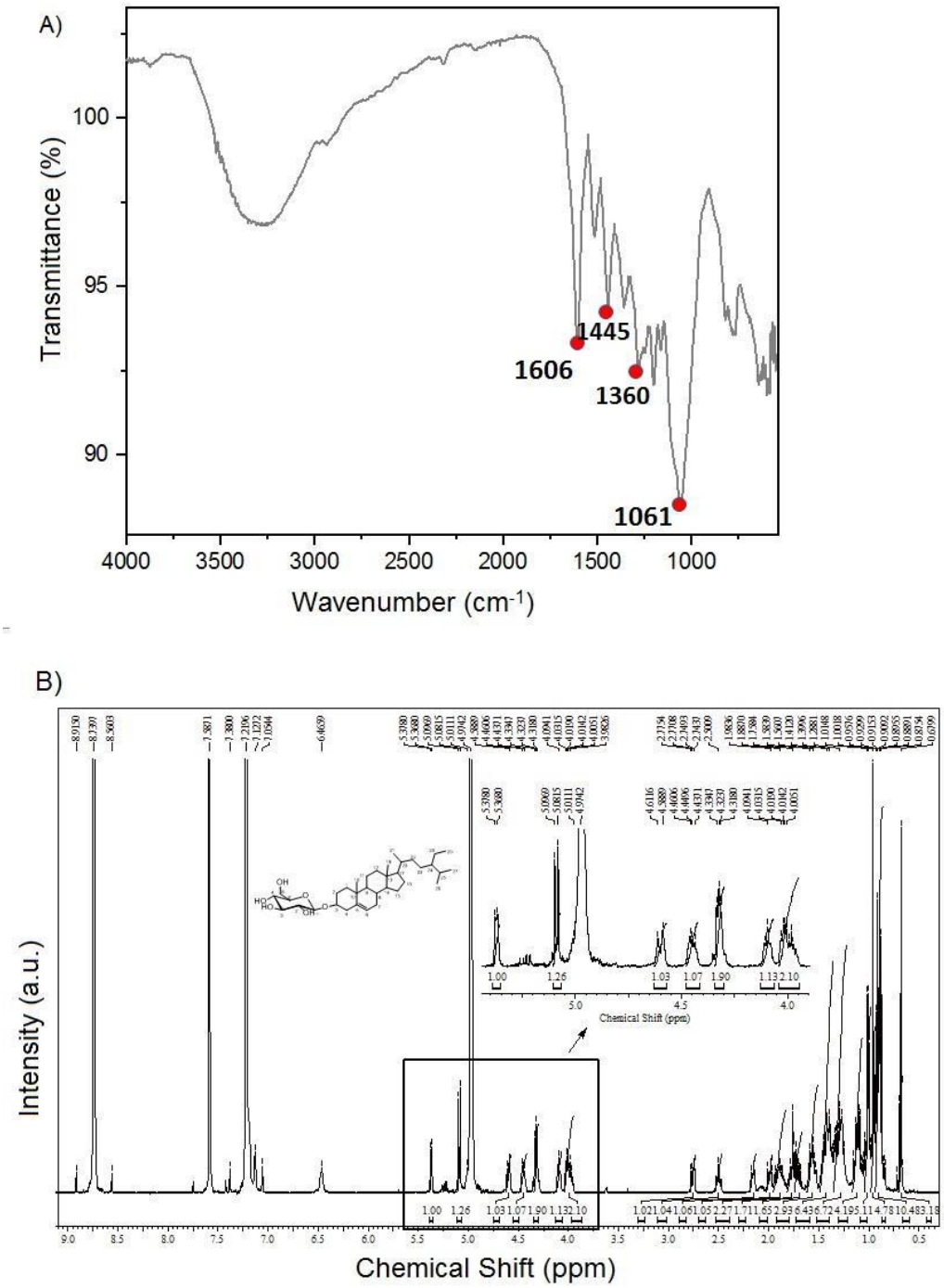

Source: Research Data (2022).

From NMR 13C spectra (Figure 2A-C) it was possible to obtain the following signals [125 MHz, Pyridine-d 5 , δ (ppm)]: 37.9 (C-1), 30.7 (C-2), 78.5 (C-3), 39.8 (C-4), 141.3 (C-5), 122.3 (C-6), 32.6 (C-7), 32.5 (C-8), 50.8 (C-9), 37.4 (C-10), 21.7 (C-11), 40.4 (C-12), 42.9 (C-13), 57.3 (C-14), 24.9 (C-15), 29.0 (C-16), 56.7 (C-17), 12.4 (C-18), 19.6 (C-19), 36.8 (C-20), 19.4 (C-21), 34.6 (C-22), 26.8 (C-23), 46.5 (C-24), 30.4 (C-25), 19.8 (C-26), 20.4 (C-27), 23.8 (C-28), 12.6 (C-29), 103.0 (C-1'), 75.8 (C-2'), 79.1 (C-3'), 72.1 (C-4'), 78.9 (C-5'), 63.3 (C-6'). The signals at δC 141,3 (C5) e 122,3 (C-6) are typical of double-bond carbons while the signals of carbonyl carbons from the glycosidic unit are found at δC 63,3 (C-6'), 78,9 (C-5'), 72,1 (C-4'), 79,1 (C-3'), 75,8 (C-8') and 103,0 (C-1') which can attributed to anomeric carbon (Ismaeel et al., 2020). Based on the ^{1}H-NMR and 13C-NMR data discussed it can be inferred that the extract is composed primarily of a mixture of steroids. These include the main component β-sitosterol and to a lesser extent Estigmasterol.

Figure 2. Expansion of the 13 C NMR observed for the ethyl acetate extract of *Rhamnidium elaeocarpum*, 2A (141.38 ppm – 72.18 ppm), 2B (63.32 ppm – 34.68 ppm), 2C (32.65 ppm – 12.44 ppm), inset of 2A: molecular structure of the main component.

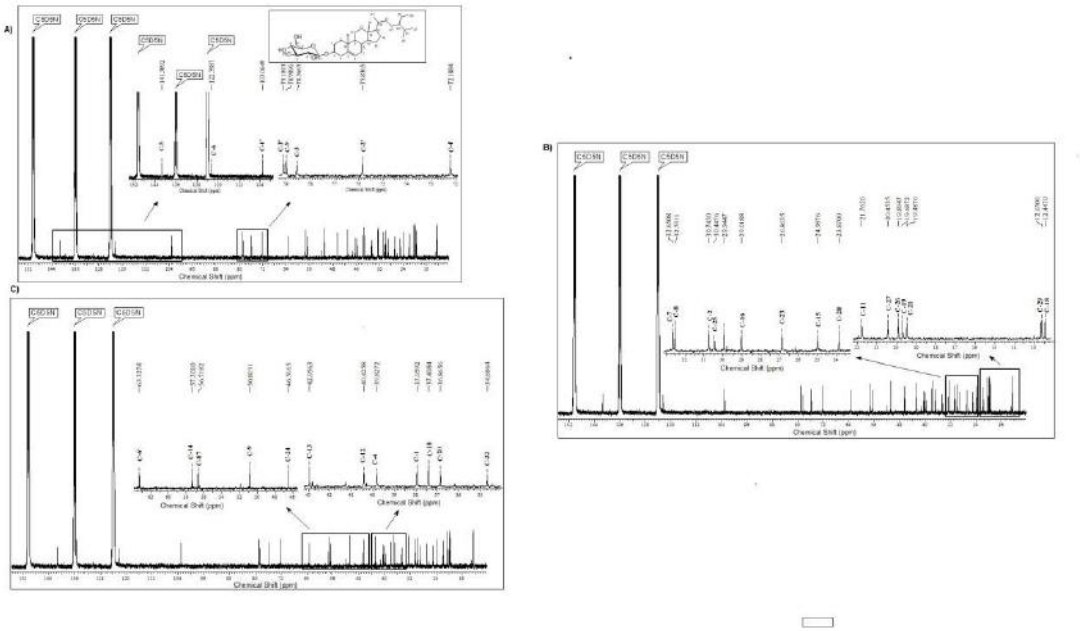

Source: Research Data (2022).

Glycoside compounds are known to function as both the reducing agent of a nanoparticle precursor as well as the stabilizing agent of metal nanoparticles. Recently, β-sitosterol glycolyzed has been reported in several screening studies for the synthesis of Ag nanoparticles (Al-Nuairi et al., 2020; Ayaz Ahmed et al., 2014; Raj R et al., 2020). In addition, other saponins bearing specific moieties have also been used as bioreducing agents in the synthesis of other metal nanoparticles. Gaikwad et al., (2019) employed the extract of *Acacia concinna willd* (Fabaceae) in the reduction of palladium nanoparticle precursors and found that the aqueous extract of the plant was mainly composed of terpenoid saponins with hydroxyl groups in their structure. The extract was used in the bioreduction of $Pd(OAc)_2$ for the manufacture of nanoparticles with an average diameter of 20 nm (Gaikwad et al., 2019).

X-ray photoelectronic spectroscopy (XPS) is a suitable technique for identifying the elements present on the material surface and their chemical states. The Survery XPS spectrum of the Fe_3O_4@ZnO-Pd catalyst is shown in 3A, from which it is possible to identify Zn, O, C and Pd as the main elements related to the composition of the material. Surface palladium

concentration obtained by XPS is ~0.43% and its peaks at 342.2 and 337.0 eV (Figure 3B) can be attributed to Pd 3d 3⁄2 and Pd 3d 5⁄2 for Pd(0) (Cao et al., 2019). It is worth mentioning that metallic palladium (Pd^0) has a characteristic binding energy ~340 and ~335 eV when supported freely on a metal oxide (Li et al., 2017; Peng et al., 2015). However, part of the metallic palladium can be bonded to O atoms of the support, and such event can explain the observed energy shift (342.2 and 337.0 eV). This effect has been reported in previous studies on supported palladium nanoparticles, including ZnO@Pd (Moon et al., 2010; Rajeswari and Gurumallesh Prabu, 2020). No Fe XPS peak was detected for this material, indicating that the magnetite nanoparticles are well-covered by the ZnO coating. This can be explained in terms of surface sensitivity of about 10 nm of XPS. Figure 3C shows the Zn2p spectrum and its binding energy peaks at 1045.3 and 1022.0 eV can be attributed to the 2p ½ and 2p 3⁄2 oxidation states, respectively, and confirm the formation of ZnO (Khataee et al., 2014; Ökte, 2014).

Figure 3. (A) survey XPS spectra, (B) Pd 3d, (C) Zn 2p, (D) C 1s and (E) O 1s spectra of Fe_3O_4@ZnO-Pd.

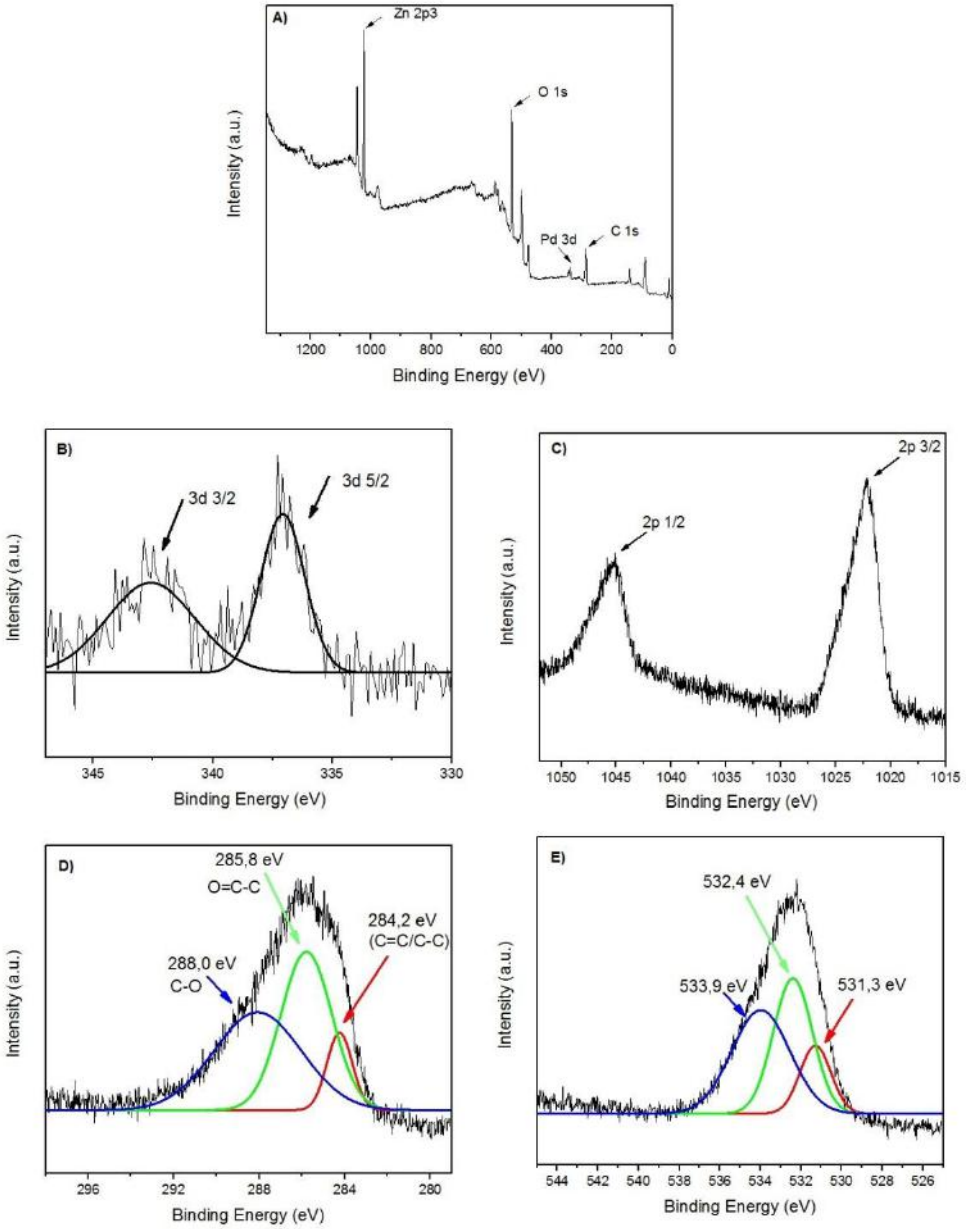

Source: Research Data (2022).

XPS C1s spectrum (Figure 3D) is deconvoluted into three peaks centered at 284.2, 285.8, and 288.0 eV. The peak at 284.2 eV is attributed to C-C sp^2 bond, whereas the remaining energies at 285.8 and 288.0 eV are assigned to carbon atoms from carboxylic (O=C-C) and hydroxyl groups (C-O), respectively (Odoom-Wubah et al., 2019). The presence of such organic groups is related to the biosynthesis approach that makes use of plant extract that contain a variety of metabolites. The fact that such organic moieties can still be detected after the subsequent washing of the catalyst indicates that the surface Pd nanoparticles are anchored to these metabolites through a chemical bridge which suggests that these particles are highly stabilized by the compounds of the ethyl acetate extract. Regarding the oxygen chemical states (Figure 3E), three distinct peaks at 531.3, 532.4, and 533.9 eV could be observed (Figure 3E). In general, oxygen bound to Zn-O crystal structures has a binding energy close to 530.0 eV. However, these binding energies can shift to higher values when a metal is anchored to the surface of the ZnO crystal lattice. This energy shift is demonstrated by Ökte in a study using lanthanide metals supported on zinc oxide (Ökte, 2014). Another study reported by Liqiang et al., on the deposition of palladium on the surface of Zn-O, demonstrates the direct relationship in the increase in binding energy for O1s species (Liqiang et al., 2004). From what has been discussed, the binding energy of 531.3 eV can be attributed to the Zn-O bond, while the peak at 532.0 eV is related to the oxygen chemisorption property (Gupta et al., 2019). Finally, the binging energy at 533.9 eV is related to Pd-O bond (Kibis et al., 2009) and it corroborates the energy shift, when compared to Pd(0) state, for the palladium spectrum (Figure 3B). For the determination of morphological and compositional profile of Fe_3O_4@ZnO-Pd, the analysis of TEM and EDS were performed. Figure 4A shows a typical TEM image in dark-field mode from which it is possible to identify bright magnetite nanocrystals surrounded by an amorphous material that corresponds to ZnO. An enlarged micrograph of the material is also shown in Figure 4B, in which the compositional determination is carried out by EDS spectroscopy (Figure 4C) of the red box area of Figure 4B. EDS analysis reveals the presence of Zn and Pd and confirms that the material was successfully fabricated. However, TEM does not show a clear contrast between the Pd nanoparticles and the ZnO layer. This has been reported before for Pd-ZnO and it is probably associated with the low atomic number contrast between Pd and Zn (Bankar et al., 2020; Barrios et al., 2015; Cable and Schaak, 2007).

Figure 4. TEM image of Fe_3O_4@ZnO-Pd (4A-B) and EDS analysis (4C) of selected area (red box from 4B).

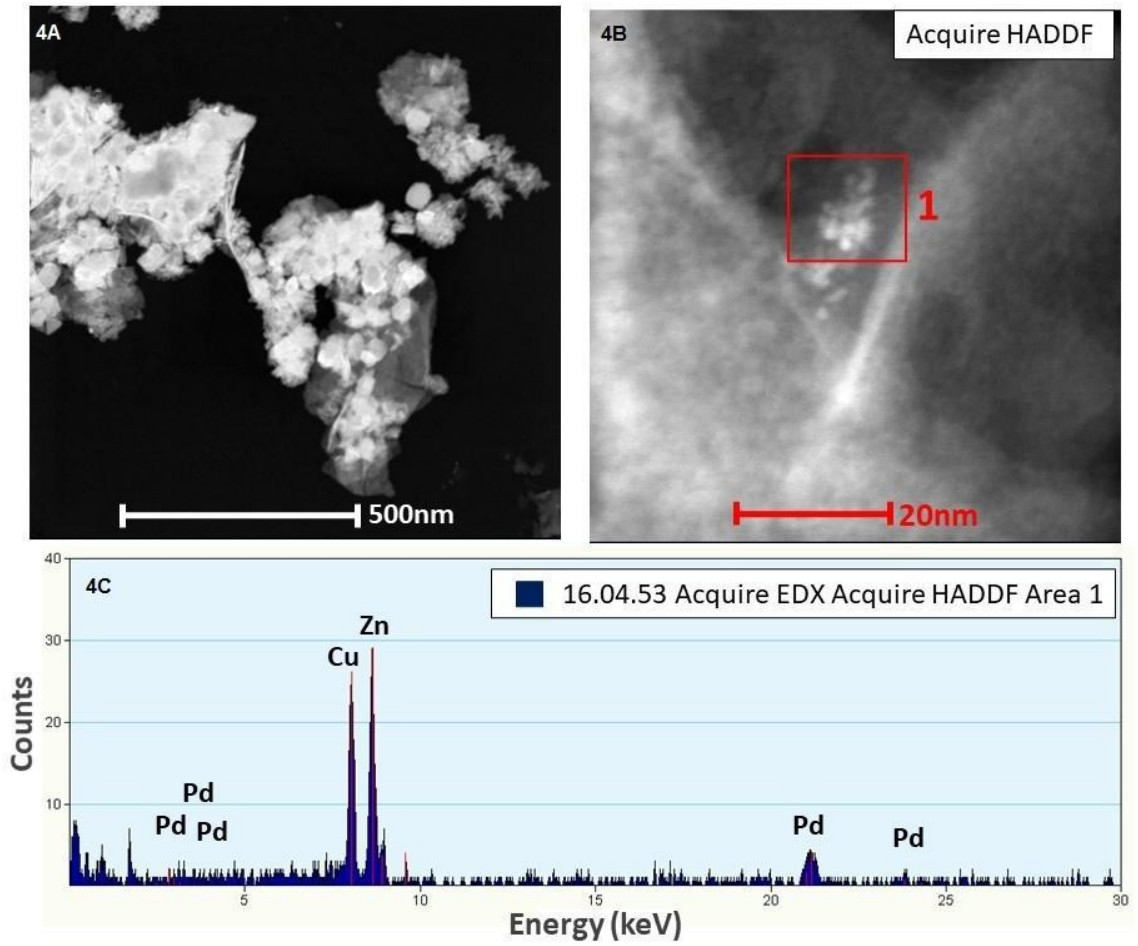

Source: Research Data (2021).

In order to better elucidate the morphology and composition of the Pd nanostructures, TEM micrographs of the biosynthesized Pd nanoparticles were also obtained prior the immobilization step. Figure 5A shows a typical TEM image of freshly prepared Pd nanoparticles of spherical shape. The size particle distribution in given in Figure 5B. The average particle diameter was found to be 3.19 nm.

Figure 5. TEM and EDS analyses for Pd nanoparticles. 5A- A TEM image of the biosynthesized Pd nanoparticles, 5B- Histogram of the Pd particle size distribution. 5C EDS analysis of 5A.

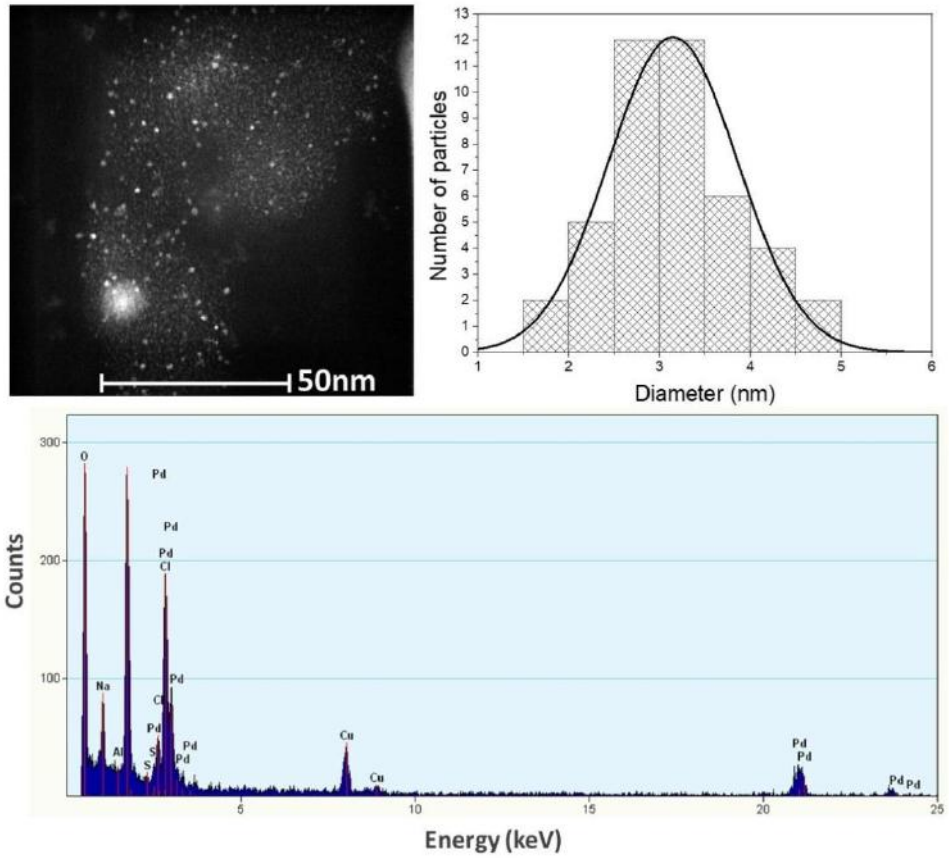

Source: Research Data (2021).

Elemental composition obtained by EDS spectroscopy (Figure 5C) confirms the formation of Pd nanoparticles with an optical absorption peak close to 2.8 keV (Cristoforetti et al., 2011). Chlorine and oxygen peaks are also present and can be related to organic groups from the biological substrate. Figure 6 shows the magnetic behavior of Fe_3O_4@ZnO-Pd obtained by VSM from which a Magnetization Saturation (Ms) of 26.8 emu g^{-1} was obtained. The material responds rapidly to an applied magnetic field and can be efficiently collected from liquid systems. It is also worth mentioning that the magnetization curve has a S-like shape with negligible coercivity. These features are consistent with a superparamagnetic behavior and are of great interest in the application of heterogeneous magnetic catalysts in liquid systems.

Figure 6.VSM magnetization curve for Fe_3O_4@ZnO-Pd.

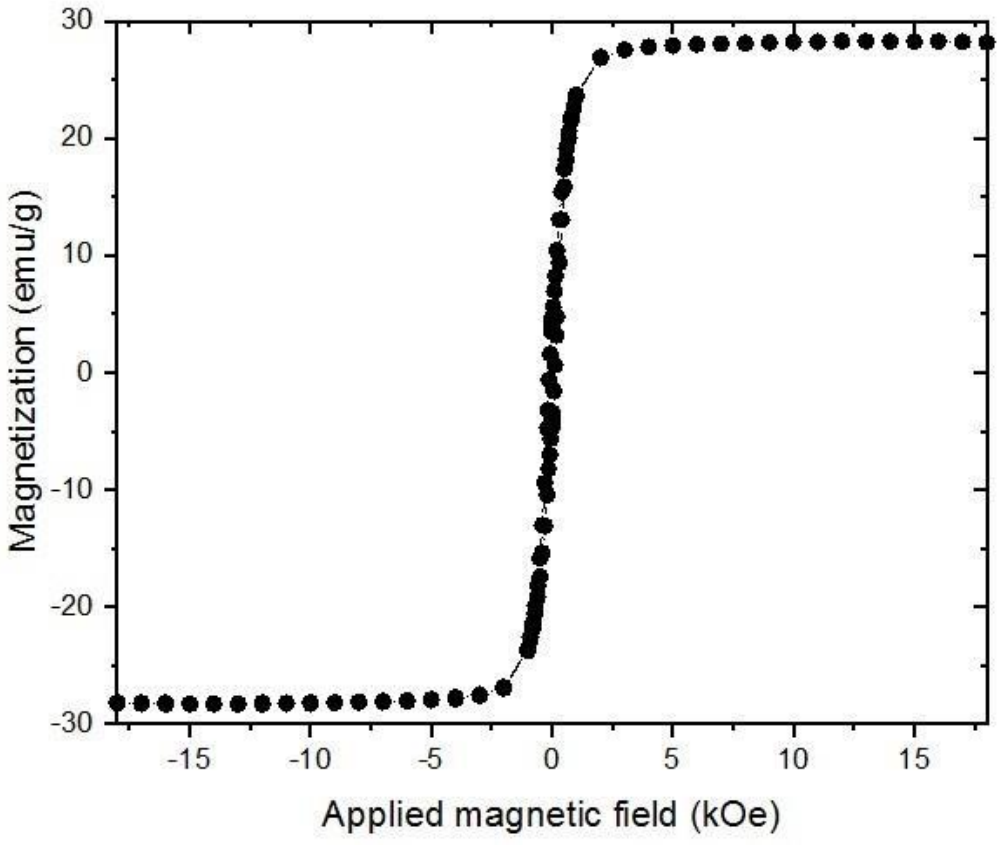

Source: Research Data (2021).

The catalytic activity of the material was initially investigated in the green oxidation of benzyl alcohol using O_2 as oxidizing agent. The optimum conditions for an active catalyst are usually those that provide the best yield. The yield is given by the product of the substrate conversion and selectivity to the target (benzaldehyde, in this study). Figure 7A shows the benzaldehyde conversion and selectivity as a function of temperature for biosynthesized catalyst. Overall, the material exhibits prominent catalytic activity towards the oxidation of benzyl alcohol, and the highest yield rate of 35.1% is achieved at 140 °C with a conversion and selectivity of 79.6% and 44%, respectively. It can also be noted that as the temperature increase the substrate conversion (benzyl alcohol) also increases but the selectivity towards the formation of benzaldehyde decreases. This behavior has been reported before and can be explained considering the thermodynamics of the reaction (Galvanin et al., 2018). The influence of O_2 pressure was also assessed, and as shown in Figure 7B increasing O_2 pressure reduces the selectivity of Benzaldehyde, going from 55.8% at 1 atm to 27.4% at 4 atm. On the other hand, the substrate conversion takes the opposite directions and increases, at a lower rate, from 68.9% at 1 atm to 89.5 at 4 atm. The fall in selectivity for higher O_2 pressure has to do with the shift of selectivity to the formation of benzoic acid as has been reported by Batista et al. The fact that our catalyst shows an optimum selectivity at low O_2 pressures and temperatures has a strong green chemistry aspect as the use of mild temperatures and gas pressures increase energy efficiency and meet the green chemical requirement needs.

Figure 7. Conversion and selectivity for benzyl alcohol oxidation to benzaldehyde and the effect of temperature (7A) and O_2 pressure (7B). reaction conditions: 1 ml of BzOH; 20 mg of catalyst; T= 140 °C; t = 60 min.

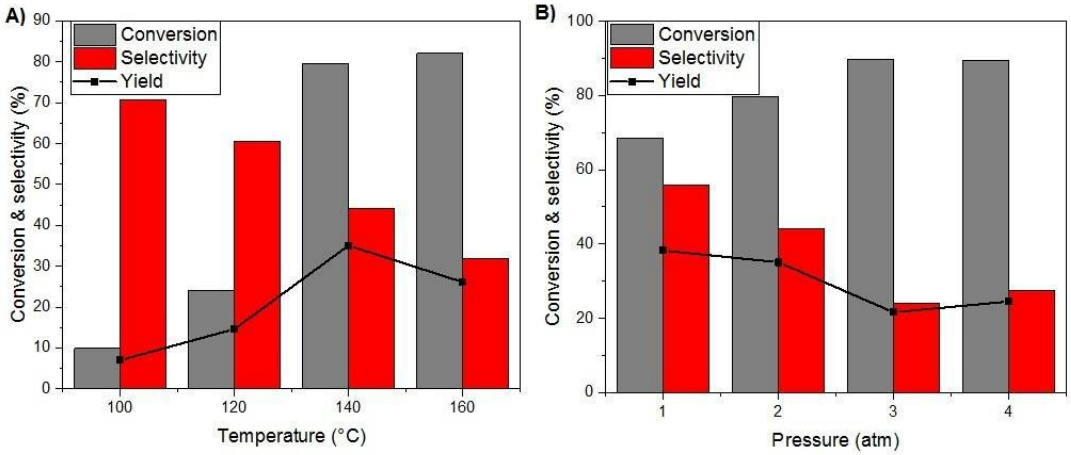

Source: Research Data (2022).

Next, the substrate/catalyst ratio was also evaluated. For this study, temperature and pressure conditions that provided the highest yield were chosen. Figure 8A exhibits the results obtained when the amount of catalyst is increased. It is very clear that by adding more catalyst to the reaction medium a decrease in selectivity is observed, and it drops from 65.2% to 36.9% when the catalyst amount is increased from 10 to 40 mg. In the opposite direction, the conversion increases substantially when a greater amount of catalyst is used ranging from 48.7% to 82.7% as the catalyst amount varies from 10 to 40 mg. In this regard, the highest yield rate is attained using 20 mg of catalyst when 68.4% of conversion and 55.9% of selectivity to benzaldehyde are found.

Figure 8. (A) Catalyst concentration study, and (B) time dependence of activity of Fe_3O_4@ZnO-Pd- reaction conditions: 1 ml of BzOH; temperature 140 °C; 1 atm (O_2), (C-D) GC-MS chromatograms and the corresponding mass spectra of the main peaks after 20 and 40 minutes of reaction, respectively.

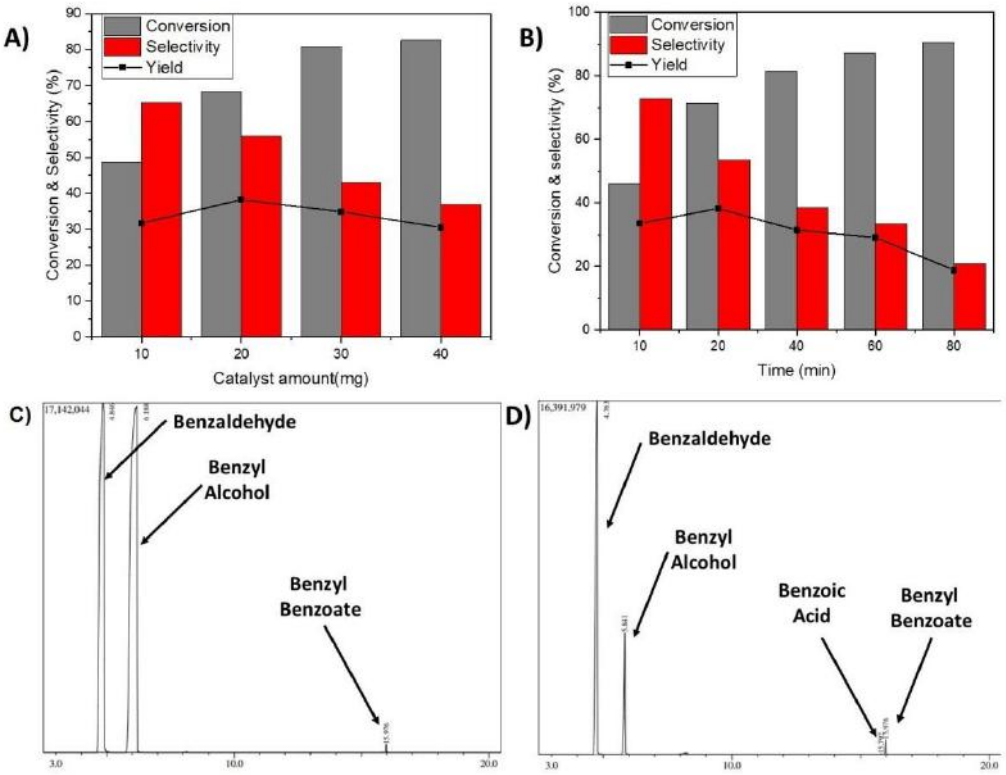

Source: Research Data (2022).

Selectivity and conversion are usually time dependent and in order to investigate its influence on the oxidation rate, several reactions with different time intervals were also carried out. Figure 8B exhibits the reaction how the selectivity and conversion of the catalytic system change as the reaction time is increases by ten minutes for each successive reaction. The highest yield (38.2 %) is achieved after 20 minutes when 71.3% of conversion and 53.5% of selectivity are observed. A GC-MS analysis was carried out to investigate the chemical composition of the by-products at 20 and 40 minutes. As can be seen in the chromatogram given in Figure 8C, benzaldehyde is the main product after 20 minutes of reaction. Moreover, there is a small concentration of benzyl benzoate. When the reaction time is increased to 40 minutes (Figure 8D), traces of benzoic acid are also identified but benzaldehyde is still detected as the main component. A catalyst recycling study was conducted in order to determine the catalyst lifespan in the oxidation of benzyl alcohol. For this purpose, reaction parameters such as the temperature, catalyst amount, O_2 pressure and reaction time were chosen based on the optimization process described before, seeking to ensure that the highest yield could be obtained. This step was also important to investigate the feasibility of catalyst recovery by a magnetic field in the reaction medium. Figure 9 shows how yield, substrate conversion and selectivity to benzaldehyde change depending on successive cycles until a partial catalyst deactivation become evident. After each reaction run, the catalyst was magnetically collected in between batches by placing small Nd magnet (4000 G) on the reactor wall. The liquid phase was removed and analyzed by HPLC. It is clear that the catalyst is highly stable throughout the oxidation of benzyl alcohol in successive runs, and an average yield as high as 45.4% was obtained up to the 8^{th} cycle. Morevover, an average conversion of 81.6% was observed for the first six runs. After the 10^{th} run the conversion drops to 31.8% but the

selectivity to benzaldehyde is still quite high. This behavior is linked to what was described before in the temperature/time studies that clearly shows that an increase in conversion leads to a reduction in selectivity.

Figure 9. Catalyst recycling for benzyl alcohol oxidation. Reaction conditions: 1 mL of BzOH; catalyst 20 mg; temperature 140 °C; 1 atm (O_2); 60 min.

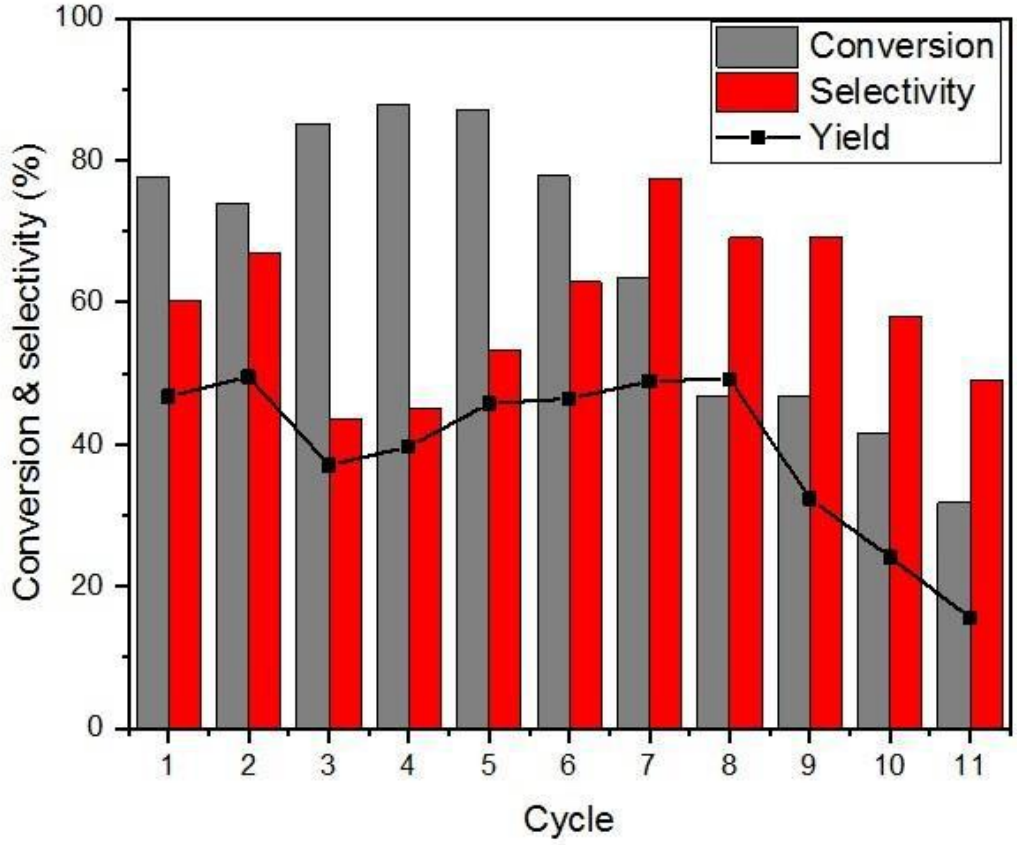

Source: Research Data (2022).

Table 1 provides catalytic data for oxidation of benzyl alcohol of other palladium based catalysts in comparison to the results obtained in this work. TOF as high as 13,686 h-1 at 140 °C was obtained for Fe_3O_4@ZnO-Pd catalyst which is quite competitive among similar reported Pd-based catalysts. However, when compared to Pd-catalysts based on bimetallic structures such as Au-Pd, Fe_3O_4@ZnO-Pd exhibits a lower TOF. The presence of a second metal such as gold tend to increase the TOF as in the case of Pd/CeO_2 catalyst (Table 1, entry 03). Overall, though, the yield found in this work for Fe_3O_4@ZnO-Pd was only lower than Au-Pd/TiO_2-rutile catalyst when compared to the data from table 1. Thus, it can be stated that the green strategy for the biosynthesis of magnetic supported Pd nanoparticles shown here allows the production of an oxidation catalyst whose efficiency and stability are comparable to those obtained by conventional methods.

Table 1. Catalytic performance of Pd based catalysts.

#	Catalyst	Selectivity (%)	Yield (%)	Reaction Temperature (°C)	Reaction Time (h)	TOF (h^{-1})	Refs.
1	Fe_3O_4@ZnO-Pd	60,23	46,78	140	0,33	13 686	This work
2	Sol-Pd/LDH-Et	98,4	12,2	140	1	11 590	[41]
3	Pd/CeO_2	98,8	12,6	160	1	16 522	[42]
4	Au-Pd/TiO_2-rutile	74,9	48,8	120	3	18 809	[43]
5	Au-Pd/TiO_2	70,0	19,3	140	0,5	20 480	[44]

Source: Data collected from references provided on Table 1.

The catalyst was also applied in the hydrogenation of alkenes and nitrocompounds, using cyclohexene and 4-nitrophenol as model compounds. Hydrogenation experiments were carried out under environmentally friendly conditions using molecular H_2 as the hydrogen source in mild temperature (75 °C) and pressure. Figure 10A shows how the reduction of cyclohexene proceeds over time. After 30 minutes of reaction, 99% of cyclohexene is converted into cyclohexane, in solventless conditions, which suggests that the catalyst exhibits a high activity for the reduction of this type of olefin. A similar behavior is observed when Fe_3O_4@ZnO-Pd is employed to reduce a nitro group to an amine (Figure 10B), and after 30 minutes of reaction at least 96% of 4-nitrophenol from the original solution is converted into 4-aminophenol. The recycling stability of Fe_3O_4@ZnO-Pd in the hydrogenation of 4-nitrophenol and cyclohexene was also investigated. Under the conditions described in Figure 9 C-D, a single sample of Fe_3O_4@ZnO-Pd could be successfully reused for more than 16 times for the reduction of cyclohexene, and an average conversion of 94% was obtained. As for the 4-nitrophenol hydrogenation, the catalyst could be reused for 20 times (average conversion of 94%). Both materials were also rapidly recovered by magnetic separation using a small Nd magnet in contact with the reactor glass wall.

Figure 10. Catalytic hydrogenation over time for Cyclohexene (10A) and 4-Nitrophenol. (10B), and recycling study for cyclohexene (10C) and 4-Nitrophenol (10D). Reaction conditions: catalyst 50 mg for cyclohexene reaction and 40 mg for 4-NP; 75 °C; PH_2 6 atm; 30 min.

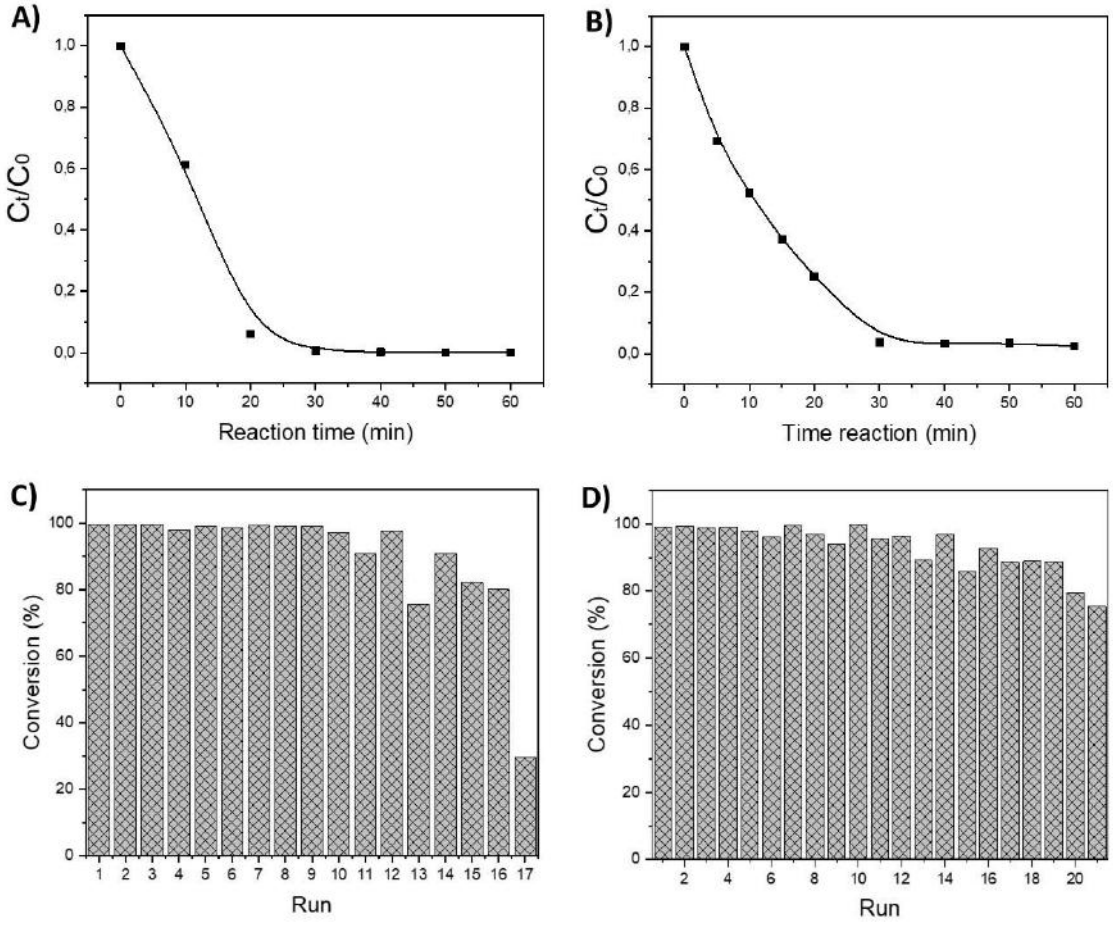

Source: Research Data (2022).

When compared to other Pd catalytic systems the results for hydrogenation of nitrocompounds and olefins obtained in the present study, using the biosynthesized magnetic Pd catalyst, are considered prominent. For comparison purposes, Table 2 exhibits catalytic data regarding efficiency and recycling of Pd catalysts published in the literature (note that experimental conditions may vary). TOF as high as 9,519.8 h^{-1} was found for cyclohexene hydrogenation using Fe_3O_4@ZnO-Pd, and this is quite impressive when compared to conventional catalytic supports for hydrogenation reactions such as SiO_2 (Table 2, entries 3 and 4). A similar conclusion can be drawn based on the catalytic data for the hydrogenation of 4-nitrophenol, and as far as TOF is considered Pd@CCTP (Table 2, entry 9) is the only catalyst whish shows a superior value. Regarding the total turnover number (TTON), which is defined as the sum of the number of mols of substrate converted into products (until catalyst deactivation) divided by the number of mols of catalyst, Fe_3O_4@ZnO-Pd exhibits a TTON of 73,934.9 and 1,659 for the hydrogenation of cyclohexene and 4-nitrophenol, respectively. These results are remarkable when contrasted to other Pd catalysts. Higher TOF and TTON can also be achieved when more drastic sources of H atoms are used such as $NaBH_4$ (Table 2, entry 9). However, using H_2 maximizes atom-use efficiency and does not generate waste which is a necessary step forward in producing greener chemicals.

Table 2. Catalytic performance of Pd based catalysts on the hydrogenation of cyclohexene and 4-nitrophenol.

#	Catalyst	Substrate	Conv. (%)	Reuses	Conditions	time (min)	TOF (h^{-1})	TON	TTON	Refs.
1	Fe_3O_4@ZnO-Pd	cyclohexene	>99	17	6 atm (H_2), 75 °C	30	9.519	4.759	73.934	This work
2	Superparamagnetic nanoparticle-supported palladium	cyclohexene	>99	20	6 atm (H_2), 75 °C	13	11.500	2500	50.000	[45]
3	SiO_2-ThiophPd(II)	cyclohexene	>99	10	10 atm (H_2), 75 °C	180	1.659	4.976	49.760	[46]
4	FFSiNH_2Pd	cyclohexene	100	10	6 atm (H_2), 75 °C	36	8.000	2.500	25.000	[47]
5	Fe_3O_4@PDA@POP@Pd-2.5%	cyclohexene	100	-	1atm (H_2), 25 °C	30	212	-	-	[48]
6	Fe_3O_4@ZnO-Pd	4-Nitrophenol	>99	21	6 atm (H_2), 75 °C	32	167	83	1.659	This work
7	Fe_3O_4@PDA@POP@Pd-2.5%	4-Nitrophenol	100	10	1 atm (H_2), 25 °C	120	52	106	1.060	[48]
8	Pd@toluene@Co/C	4-Nitrophenol	>99	6	1 atm (H_2), 50 °C	60	100	98	588	[49]
9	Pd@CCTP	4-Nitrophenol	>99	9	$NaBH_4$, 50°C	7	883	555	4.995	[50]

Source: Data collected from references provided on Table 2.

4. Conclusion

The bark/stem extract of *R. elaeocarpum* species has been successfully employed as reducing/capping agents of Pd nanoparticles. The biosynthetic protocol allowed the the synthesis of ~ 21.9 nm nanoparticles which were deposited on the surface of the magnetic composite (Fe_3O_4@ZnO). The superparamagnetic behavior of the material allowed it to be quickly dispersed in liquid medium which is also fundamental for a heterogeneous catalyst in liquid systems containing the target substrates. The catalyst was applied in the oxidation of alcohol and hydrogenation as nitrocompounds using, respectively, benzyl alcohol and cyclohexene as model substrates. TOF as high as 13,686 h^{-1} was achieved for the oxidation of benzyl alcohol in solventless conditions. Not only is this result competitive with that of other Pd based catalysts, but it also stands out among other bimetallic Pd-catalysts. During the recycling studies, it was observed that an average yield rate of 45.5% could be achieved for the first eight runs, and an average conversion of 81.6% was also obtained for the first six cycles. The material was also applied in the hydrogenation of 4-nitrophenol and cyclohexene, and a conversion higher than 96% was obtained after 30 minutes of reaction. For the catalyst recycling in the hydrogenation of 4-nitrophenol, an even higher recycling capability was observed and on portion could be reused for 21 times (average conversion higher than 94%). FTIR and NMR analyses showed that the biological extract s is mainly composed of β-sitosterol and Estigmasterol that can efficiently stabilize the Pd nanoparticles. We believe that the methodology presented in this work adds important contribution towards the fabrication of multifunctional hybrid materials combining biosynthesis and friendly synthetic methodologies.

Acknowledgments

The authors are grateful to Fundação de Amparo à Pesquisa do Estado de Mato Grosso (FAPEMAT) and Conselho Nacional de Desenvolvimento Científico e Tecnológico (CNPq) for financial support, and indebted to LCE-DEMA-UFSCAR for TEM and FTIR analyses, respectively. We also thank Coordenação de Aperfeiçoamento de Pessoal de Nível Superior—Brasil (CAPES, Finance Code: 001).

References

Al-Nuairi, A. G., Mosa, K. A., Mohammad, M. G., El-Keblawy, A., Soliman, S., & Alawadhi, H. (2020). Biosynthesis, Characterization, and Evaluation of the Cytotoxic Effects of Biologically Synthesized Silver Nanoparticles from Cyperus conglomeratus Root Extracts on Breast Cancer Cell Line MCF-7. *Biological Trace Element Research, 194(2), 560–569*. https://doi.org/10.1007/s12011-019-01791-7

Ammar, S. H., Abdulnabi, W. A., & kader, H. D. A. (2020). Synthesis, characterization and environmental remediation applications of polyoxometalates-based magnetic zinc oxide nanocomposites (Fe3O4@ZnO/PMOs). *Environmental Nanotechnology, Monitoring & Management, 13, 100289*. https://doi.org/https://doi.org/10.1016/j.enmm.2020.100289

Ayaz Ahmed, K. B., Subramaniam, S., Veerappan, G., Hari, N., Sivasubramanian, A., & Veerappan, A. (2014). β-Sitosterol-d-glucopyranoside isolated from Desmostachya bipinnata mediates photoinduced rapid green synthesis of silver nanoparticles. *RSC Advances, 4(103), 59130–59136*. https://doi.org/10.1039/C4RA10626A

Bahruji, H., Bowker, M., Hutchings, G., Dimitratos, N., Wells, P., Gibson, E., Jones, W., Brookes, C., Morgan, D., & Lalev, G. (2016). Pd/ZnO catalysts for direct CO2 hydrogenation to methanol. *Journal of Catalysis, 343, 133–146*. https://doi.org/https://doi.org/10.1016/j.jcat.2016.03.017

Bahtiar, S., Taufiq, A., Utomo, J., Hidayat, N., & Sunaryono, S. (2019). Structural Characterizations of Magnetite/Zinc Oxide Nanocomposites Prepared by Co-precipitation Method. *IOP Conference Series: Materials Science and Engineering, 515, 12076*. https://doi.org/10.1088/1757-899X/515/1/012076

Bankar, D. B., Hawaldar, R. R., Arbuj, S. S., Shinde, S. T., Gadde, J. R., Rakshe, D. S., Amalnerkar, D. P., & Kanade, K. G. (2020). Palladium loaded on ZnO nanoparticles: Synthesis, characterization and application as heterogeneous catalyst for Suzuki–Miyaura cross-coupling reactions under ambient and ligand-free conditions. *Materials Chemistry and Physics, 243, 122561*. https://doi.org/https://doi.org/10.1016/j.matchemphys.2019.122561

Barrios, C. E., Bosco, M. V, Baltanás, M. A., & Bonivardi, A. L. (2015). Hydrogen production by methanol steam reforming: Catalytic performance of supported-Pd on zinc–cerium oxides' nanocomposites. *Applied Catalysis B: Environmental, 179, 262–275*. https://doi.org/https://doi.org/10.1016/j.apcatb.2015.05.030

Batista, F. R. M., da S. Melo, I. E. M., dos Santos Pereira, L., Lima, A. A. G., Bashal, A. H., Costa, J. C. S., Magalhães, J. L., Lima, F. C. A., de Moura, C., Garcia, M. A. S., & de Moura, E. M. (2020). Screening of the Au:Pt Atomic Ratio Supported in SrCO3: Effects on the Performance of the Solvent-Free Oxidation of Benzyl Alcohol. *Journal of the Brazilian Chemical Society, 31, 488*. https://doi.org/https://doi.org/10.21577/0103-5053.20190207

Cable, R. E., & Schaak, R. E. (2007). Solution Synthesis of Nanocrystalline M−Zn (M = Pd, Au, Cu) Intermetallic Compounds via Chemical Conversion of Metal Nanoparticle Precursors. *Chemistry of Materials, 19(16), 4098–4104*. https://doi.org/10.1021/cm071214j

Camargo, P., Satyanarayana, K. G., & Wypych, F. (2009). Nanocomposites: Synthesis, Structure, Properties and New Application Opportunities. *Materials Research-Ibero-American Journal of Materials - MATER RES-IBERO-AM J MATER*, 12. https://doi.org/10.1590/S1516-14392009000100002

Cao, P., Yang, Z., Navale, S. T., Han, S., Liu, X., Liu, W., Lu, Y., Stadler, F. J., & Zhu, D. (2019). Ethanol sensing behavior of Pd-nanoparticles decorated ZnO-nanorod based chemiresistive gas sensors. *Sensors and Actuators B: Chemical, 298, 126850*. https://doi.org/https://doi.org/10.1016/j.snb.2019.126850

Chuc, L. T. N., Chen, C.-S., Lo, W.-S., Shen, P.-C., Hsuan, Y.-C., Tsai, H.-H. G., Shieh, F.-K., & Hou, D.-R. (2017). Long-Range Olefin Isomerization Catalyzed by Palladium(0) Nanoparticles. *ACS Omega, 2(2), 698–711*. https://doi.org/10.1021/acsomega.6b00509

Cristoforetti, G., Pitzalis, E., Spiniello, R., Ishak, R., & Muniz-Miranda, M. (2011). Production of Palladium Nanoparticles by Pulsed Laser Ablation in Water and Their Characterization. *The Journal of Physical Chemistry C, 115(12), 5073–5083*. https://doi.org/10.1021/jp109281q

da Silva, F. P., Fiorio, J. L., & Rossi, L. M. (2017). Tuning the Catalytic Activity and Selectivity of Pd Nanoparticles Using Ligand-Modified Supports and Surfaces. *ACS Omega, 2(9), 6014–6022*. https://doi.org/10.1021/acsomega.7b00836

da Silva, R. A., Jacinto, M. J., Silva, V. C., & Cabana, D. C. (2018). Urea-assisted fabrication of Fe3O4@ZnO@Au composites for the catalytic photodegradation of Rhodamine-B. *Journal of Sol-Gel Science and Technology, 86(1), 94–103*. https://doi.org/10.1007/s10971-018-4607-0

Gaikwad, D. S., Undale, K. A., Kalel, R. A., & Patil, D. B. (2019). Acacia concinna pods: a natural and new bioreductant for palladium nanoparticles and its application to Suzuki–Miyaura coupling. *Journal of the Iranian Chemical Society, 16(10), 2135–2141*. https://doi.org/10.1007/s13738-019-01682-7

Galvanin, F., Sankar, M., Cattaneo, S., Bethell, D., Dua, V., Hutchings, G. J., & Gavriilidis, A. (2018). On the development of kinetic models for solvent-free benzyl alcohol oxidation over a gold-palladium catalyst. *Chemical Engineering Journal, 342, 196–210*. https://doi.org/https://doi.org/10.1016/j.cej.2017.11.165

Guo, Y., Gao, Y., Li, X., Zhuang, G., Wang, K., Zheng, Y., Sun, D., Huang, J., & Li, Q. (2019). Catalytic benzene oxidation by biogenic Pd nanoparticles over 3D-ordered mesoporous CeO2. *Chemical Engineering Journal, 362, 41–52*. https://doi.org/https://doi.org/10.1016/j.cej.2019.01.012

Gupta, S. P., Pawbake, A. S., Sathe, B. R., Late, D. J., & Walke, P. S. (2019). Superior humidity sensor and photodetector of mesoporous ZnO nanosheets at room temperature. *Sensors and Actuators B: Chemical, 293, 83–92*. https://doi.org/https://doi.org/10.1016/j.snb.2019.04.086

Hu, Z., Zhou, G., Xu, L., Yang, J., Zhang, B., & Xiang, X. (2019). Preparation of ternary Pd/CeO2-nitrogen doped graphene composites as recyclable catalysts for solvent-free aerobic oxidation of benzyl alcohol. *Applied Surface Science, 471, 852–861*. https://doi.org/https://doi.org/10.1016/j.apsusc.2018.12.067

Ismaeel, S., Jaber, H., & Zayed, R. (2020). ISOLATION OF β-SITOSTEROL FROM TAMARIX *APHYLLA OF IRAQ. Biochem. Cell. Arch. 20(2), 6497–6502*. https://doi.org/https://connectjournals.com/03896.2020.20.6497

Jacinto, M. J., Souto, R. S., Silva, V. C. P., Prescilio, I. C., Kauffmann, A. C., Soares, M. A., de Souza, J. R., Bakuzis, A. F., & Fontana, L. C. (2021). Biosynthesis of Cube-Shaped Fe3O4 Nanoparticles for Removal of Dyes Using Fenton Process. *Water, Air, & Soil Pollution, 232(7), 270*. https://doi.org/10.1007/s11270-021-05233-w

Khataee, A. R., Karimi, A., Soltani, R. D. C., Safarpour, M., Hanifehpour, Y., & Joo, S. W. (2014). Europium-doped ZnO as a visible light responsive nanocatalyst: Sonochemical synthesis, characterization and response surface modeling of photocatalytic process. *Applied Catalysis A: General, 488, 160–170*. https://doi.org/https://doi.org/10.1016/j.apcata.2014.09.039

Kibis, L. S., Titkov, A. I., Stadnichenko, A. I., Koscheev, S. V, & Boronin, A. I. (2009). X-ray photoelectron spectroscopy study of Pd oxidation by RF discharge in oxygen. *Applied Surface Science, 255(22), 9248–9254*. https://doi.org/https://doi.org/10.1016/j.apsusc.2009.07.011

Kuai, L., Chen, Z., Liu, S., Kan, E., Yu, N., Ren, Y., Fang, C., Li, X., Li, Y., & Geng, B. (2020). Titania supported synergistic palladium single atoms and nanoparticles for room temperature ketone and aldehydes hydrogenation. *Nature Communications, 11(1), 48*. https://doi.org/10.1038/s41467-019-13941-5

Li, X., Feng, J., Sun, J., Wang, Z., & Zhao, W. (2019). Solvent-Free Catalytic Oxidation of Benzyl Alcohol over Au-Pd Bimetal Deposited on TiO2: Comparison of Rutile, Brookite, and Anatase. *Nanoscale Research Letters, 14(1), 394*. https://doi.org/10.1186/s11671-019-3211-8

Li, X., Zeng, Z., Hu, B., Qian, L., & Hong, X. (2017). Surface-Atom Dependence of ZnO-Supported Ag@Pd Core@Shell Nanocatalysts in CO2 Hydrogenation to CH3OH. *ChemCatChem, 9(6), 924–928*. https://doi.org/https://doi.org/10.1002/cctc.201601119

Liqiang, J., Baiqi, W., Baifu, X., Shudan, L., Keying, S., Weimin, C., & Honggang, F. (2004). Investigations on the surface modification of ZnO nanoparticle photocatalyst by depositing Pd. *Journal of Solid State Chemistry, 177(11), 4221–4227*. https://doi.org/https://doi.org/10.1016/j.jssc.2004.08.016

López-Salazar, H., Camacho-Díaz, B. H., Ávila-Reyes, S. V, Pérez-García, M. D., González- Cortazar, M., Arenas Ocampo, M. L., & Jiménez-Aparicio, A. R. (2019). Identification and Quantification of β-Sitosterol β-d-Glucoside of an Ethanolic Extract Obtained by Microwave-Assisted Extraction from Agave angustifolia Haw. *In Molecules (Vol. 24, Issue 21)*. https://doi.org/10.3390/molecules24213926

Ma, M., Yang, Y., Li, W., Feng, R., Li, Z., Lyu, P., & Ma, Y. (2019). Gold nanoparticles supported by amino groups on the surface of magnetite microspheres for the catalytic reduction of 4-nitrophenol. *Journal of Materials Science, 54(1), 323–334*. https://doi.org/10.1007/s10853-018-2868-1

Mallat, T., & Baiker, A. (2004). Oxidation of Alcohols with Molecular Oxygen on Solid Catalysts. *Chemical Reviews, 104(6), 3037–3058*. https://doi.org/10.1021/cr0200116

Miceli, M., Frontera, P., Macario, A., & Malara, A. (2021). Recovery/Reuse of Heterogeneous Supported Spent Catalysts. *Catalysts, 11(5)*. https://doi.org/https://doi.org/10.3390/catal11050591

Miedziak, P. J., He, Q., Edwards, J. K., Taylor, S. H., Knight, D. W., Tarbit, B., Kiely, C. J., & Hutchings, G. J. (2011). Oxidation of benzyl alcohol using supported gold–palladium nanoparticles. *Catalysis Today, 163(1), 47–54*. https://doi.org/https://doi.org/10.1016/j.cattod.2010.02.051

Moon, J., Park, J.-A., Lee, S.-J., Zyung, T., & Kim, I.-D. (2010). Pd-doped TiO2 nanofiber networks for gas sensor applications. *Sensors and Actuators B: Chemical, 149(1), 301–305*. https://doi.org/https://doi.org/10.1016/j.snb.2010.06.033

Munvera, A., Nyemb, J. N., Alfred Ngenge, T., Mafo, M. A. F., Nuzhat, S., & Nkengfack, A. E. (2021). First report of isolation of antibacterial ceramides from the leaves of Euclinia longiflora Salisb. *Natural Product Communications, 16(11), 1934578X211048628*. https://doi.org/10.1177/1934578X211048628

Ododo, M. M., Choudhury, M. K., & Dekebo, A. H. (2016). Structure elucidation of β-sitosterol with antibacterial activity from the root bark of Malva parviflora. *SpringerPlus, 5(1), 1210*. https://doi.org/10.1186/s40064-016-2894-x

Odoom-Wubah, T., Li, Q., Wang, Q., Rukhsana Usha, M. Z., Huang, J., & Li, Q. (2019). Template-free synthesis of carbon self-doped ZnO superstructures as efficient support for ultra fine Pd nanoparticles and their catalytic activity towards benzene oxidation. *Molecular Catalysis, 469, 118–130*. https://doi.org/https://doi.org/10.1016/j.mcat.2019.03.013

Ökte, A. N. (2014). Characterization and photocatalytic activity of Ln (La, Eu, Gd, Dy and Ho) loaded ZnO nanocatalysts. *Applied Catalysis A: General, 475, 27–39*. https://doi.org/https://doi.org/10.1016/j.apcata.2014.01.019

Parmanand, Kumari, S., Mittal, A., Kumar, A., Krishna, & Sharma, S. K. (2019). Palladium Nanoparticles Immobilized on Schiff Base-Functionalized Graphene-Oxide: Application in Carbon-Carbon Cross-Coupling Reactions. *ChemistrySelect, 4(36), 10828–10837*. https://doi.org/https://doi.org/10.1002/slct.201902242

Peng, S.-Y., Xu, Z.-N., Chen, Q.-S., Wang, Z.-Q., Lv, D.-M., Sun, J., Chen, Y., & Guo, G.-C. (2015). Enhanced Stability of Pd/ZnO Catalyst for CO Oxidative Coupling to Dimethyl Oxalate: Effect of Mg2+ Doping. *ACS Catalysis, 5(7), 4410–4417*. https://doi.org/10.1021/acscatal.5b00365

Raimundo e Silva, J. P., Policarpo, I. da S., Chaves, T. P., Coutinho, H. D. M., & Alves, H. da S. (2020). A glycosylated β-Sitosterol, isolated from Tacinga inamoena (Cactaceae), enhances the antibacterial activity of conventional antibiotics. *South African Journal of Botany, 133, 193–200*. https://doi.org/https://doi.org/10.1016/j.sajb.2020.07.017

Raj R, K., D, E., & S, R. (2020). β-Sitosterol-assisted silver nanoparticles activates Nrf2 and triggers mitochondrial apoptosis via oxidative stress in human hepatocellular cancer cell line. *Journal of Biomedical Materials Research Part A, 108(9), 1899–1908*. https://doi.org/https://doi.org/10.1002/jbm.a.36953

Rajeswari, R., & Gurumallesh Prabu, H. (2020). Palladium – Decorated reduced graphene oxide/zinc oxide nanocomposite for enhanced antimicrobial, antioxidant and cytotoxicity activities. *Process Biochemistry, 93, 36–47*. https://doi.org/https://doi.org/10.1016/j.procbio.2020.03.010

Rossi, L. M., Silva, F. P., Vono, L. L. R., Kiyohara, P. K., Duarte, E. L., Itri, R., Landers, R., & Machado, G. (2007). Superparamagnetic nanoparticle-supported palladium: a highly stable magnetically recoverable and reusable catalyst for hydrogenation reactions. *Green Chemistry, 9(4), 379–385*. https://doi.org/10.1039/B612980C

Shanmugam, P., Murthy, A. P., Theerthagiri, J., Wei, W., Madhavan, J., Kim, H.-S., Maiyalagan, T., & Xie, J. (2019). Robust bifunctional catalytic activities of N-doped carbon aerogel-nickel composites for electrocatalytic hydrogen evolution and hydrogenation of nitrocompounds. *International Journal of Hydrogen Energy, 44(26), 13334–13344*. https://doi.org/https://doi.org/10.1016/j.ijhydene.2019.03.225

Stadler, L., Homafar, M., Hartl, A., Najafishirtari, S., Colombo, M., Zboril, R., Martin, P., Gawande, M. B., Zhi, J., & Reiser, O. (2019). Recyclable Magnetic Microporous Organic Polymer (MOP) Encapsulated with Palladium Nanoparticles and Co/C Nanobeads for Hydrogenation Reactions. *ACS Sustainable Chemistry & Engineering, 7(2), 2388–2399*. https://doi.org/10.1021/acssuschemeng.8b05222

Vieira, Y., Silvestri, S., Leichtweis, J., Jahn, S. L., de Moraes Flores, É. M., Dotto, G. L., & Foletto, E. L. (2020). New insights into the mechanism of heterogeneous activation of nano–magnetite by microwave irradiation for use as Fenton catalyst. *Journal of Environmental Chemical Engineering, 8(3), 103787*. https://doi.org/https://doi.org/10.1016/j.jece.2020.103787

Wang, J., Yang, J., Li, X., Wang, D., Wei, B., Song, H., Li, X., & Fu, S. (2016). Preparation and photocatalytic properties of magnetically reusable Fe3O4@ZnO core/shell nanoparticles. *Physica E: Low-Dimensional Systems and Nanostructures, 75, 66–71*. https://doi.org/https://doi.org/10.1016/j.physe.2015.08.040

Wu, W., Zhang, S., Xiao, X., Zhou, J., Ren, F., Sun, L., & Jiang, C. (2012). Controllable Synthesis, Magnetic Properties, and Enhanced Photocatalytic Activity of Spindlelike Mesoporous α-Fe2O3/ZnO Core–Shell Heterostructures. *ACS Applied Materials & Interfaces, 4(7), 3602–3609*. https://doi.org/10.1021/am300669a

Yadav, D., & Awasthi, S. K. (2020). A Pd confined hierarchically conjugated covalent organic polymer for hydrogenation of nitroaromatics: catalysis, kinetics, thermodynamics and mechanism. *Green Chemistry, 22(13), 4295–4303*. https://doi.org/10.1039/D0GC01469A

Yang, J., Zhu, Y., Fan, M., Sun, X., Wang, W. D., & Dong, Z. (2019). Ultrafine palladium nanoparticles confined in core–shell magnetic porous organic polymer nanospheres as highly efficient hydrogenation catalyst. *Journal of Colloid and Interface Science, 554, 157–165*. https://doi.org/https://doi.org/10.1016/j.jcis.2019.07.006

Yilmaz, F. (2018). Heterogen Catalysis in Sustainable Green Solvent: Alkenes Hydrogenation With New Silica Immobilized Palladium Complex Containing S,O-Chelating Ligand. Anadolu University *Journal of Science and Technology-A Applied Sciences and Engineering, 1*. https://doi.org/10.18038/aubtda.409518

Yu, T., Jiao, J., Song, P., Nie, W., Yi, C., Zhang, Q., & Li, P. (2020). Recent Progress in Continuous-Flow Hydrogenation. *ChemSusChem, 13(11), 2876–2893*. https://doi.org/https://doi.org/10.1002/cssc.202000778

Zhang, H., Guo, W., Lu, N., & Fan, B. (2020). Solvent-free selective oxidation of aromatic alcohol with O2 over MgAl-LDH supported Pd nanoparticles: Effects of preparation methods and solvents. *Materials Chemistry and Physics, 252, 123193*. https://doi.org/https://doi.org/10.1016/j.matchemphys.2020.123193